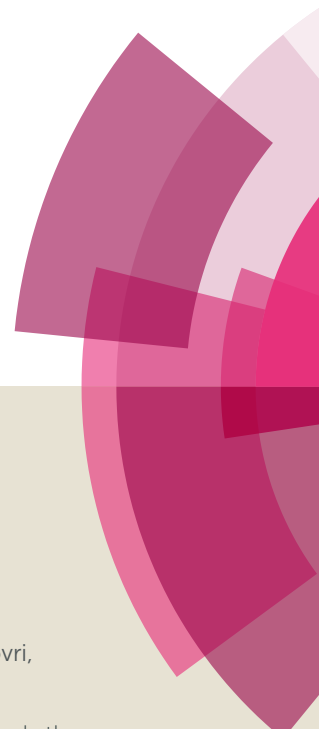


# NJC

Accepted Manuscript



This article can be cited before page numbers have been issued, to do this please use: V. Vrdoljak, B. Prugoveki, I. Primoži, T. Hrenar, D. Cvijanovi, J. Parlov Vukovi, R. Odžak, M. Skoibuši, S. Prugoveki, J. Lovri, D. Matkovi-alogovi and M. Cindric, *New J. Chem.*, 2018, DOI: 10.1039/C8NJ01457D.



This is an Accepted Manuscript, which has been through the Royal Society of Chemistry peer review process and has been accepted for publication.

Accepted Manuscripts are published online shortly after acceptance, before technical editing, formatting and proof reading. Using this free service, authors can make their results available to the community, in citable form, before we publish the edited article. We will replace this Accepted Manuscript with the edited and formatted Advance Article as soon as it is available.

You can find more information about Accepted Manuscripts in the [author guidelines](#).

Please note that technical editing may introduce minor changes to the text and/or graphics, which may alter content. The journal's standard [Terms & Conditions](#) and the ethical guidelines, outlined in our [author and reviewer resource centre](#), still apply. In no event shall the Royal Society of Chemistry be held responsible for any errors or omissions in this Accepted Manuscript or any consequences arising from the use of any information it contains.

# An integrated approach (synthetic, structural and biological) in the study of aroylhydrazone salts

Višnja Vrdoljak,<sup>\*a</sup> Biserka Prugovečki,<sup>a</sup> Ines Primožič,<sup>a</sup> Tomica Hrenar,<sup>a</sup> Danijela Cvijanović,<sup>b</sup> Jelena Parlov Vuković,<sup>c</sup> Renata Odžak,<sup>d</sup> Mirjana Skočibušić,<sup>e</sup> Stjepan Prugovečki,<sup>f</sup> Jasna Lovrić,<sup>b</sup> Dubravka Matković-Čalogović,<sup>a</sup> Marina Cindrić<sup>a</sup>

Received (in XXX, XXX) Xth XXXXXXXXX 200X, Accepted Xth XXXXXXXXX 200X

First published on the web Xth XXXXXXXXX 200X

DOI: 10.1039/b000000x

The reaction of two methoxy substituted salinazid-based hydrazones, 4-methoxysalicylaldehyde isonicotinoyl hydrazone (**L**<sup>1</sup>) and 3-methoxysalicylaldehyde isonicotinoyl hydrazone (**L**<sup>2</sup>) with HCl, HBr, HNO<sub>3</sub> and H<sub>2</sub>SO<sub>4</sub> in methanol yielded salts of different stoichiometries (1:1 or 2:1) and/or polymorphic forms. In such a way (**HL**<sup>1</sup>)<sup>+</sup>**X**<sup>-</sup> and (**HL**<sup>2</sup>)<sup>+</sup>**X**<sup>-</sup> salts where X = Cl, Br, NO<sub>3</sub>, HSO<sub>4</sub>, as well as [**H(L**<sup>1</sup>)<sub>2</sub>]<sup>+</sup>Br<sup>-</sup> and (**HL**<sup>1</sup>)<sub>2</sub><sup>+</sup>SO<sub>4</sub><sup>2-</sup> were obtained. Solid state properties and propensity for transformation between different forms in solution were also investigated. Crystal structures of compounds (**HL**<sup>1</sup>)<sup>+</sup>Cl<sup>-</sup>, (**HL**<sup>1</sup>)<sup>+</sup>Br<sup>-</sup> (**α** and **β**), [**H(L**<sup>1</sup>)<sub>2</sub>]<sup>+</sup>Br<sup>-</sup>, (**HL**<sup>1</sup>)<sub>2</sub><sup>+</sup>SO<sub>4</sub><sup>2-</sup>, (**HL**<sup>2</sup>)<sup>+</sup>Br<sup>-</sup>·MeOH and (**HL**<sup>2</sup>)<sup>+</sup>NO<sub>3</sub><sup>-</sup> were solved by the single-crystal X-ray diffraction method while structures of (**HL**<sup>1</sup>)<sup>+</sup>NO<sub>3</sub><sup>-</sup>, (**HL**<sup>1</sup>)<sup>+</sup>HSO<sub>4</sub><sup>-</sup> (**α** and **β**) were solved by the powder diffraction method. Details of anion binding with the isoniazid functionality are discussed. The aroylhydrazone salts were evaluated for cytotoxic activity *in vitro*. All compounds exhibited weak cytotoxicity against THP-1 and no cytotoxicity against HepG2 cells. In a preliminary antimicrobial screening assay, these compounds were not only active against antibiotic susceptible Gram-positive, but also exhibited antibacterial effects on a wide range of multidrug-resistant Gram-positive as well as multidrug resistant Gram-negative bacterial pathogens.

## Introduction

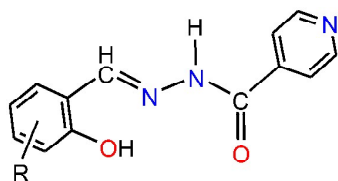
The chemistry of hydrazones has been receiving an ongoing attention in various fields, ranging from organic synthesis<sup>1-3</sup> and medicinal chemistry<sup>4-6</sup> to supramolecular<sup>7,8</sup> and coordination chemistry.<sup>9,10</sup> Structural features and unique physical and chemical properties of hydrazones determine the range of applications they can be involved in. Furthermore, the hydrazone moiety R-C=N-NH-R' can undergo reversible structural changes upon photochemical treatment and triggers like pH or temperature changes.<sup>11-15</sup> This makes the hydrazone group suitable for switching applications upon stimuli responsive *E/Z* (*anti,syn*) isomerization. This is more pronounced in the case when the R group has the hydrogen bond accepting capability.<sup>16</sup>

Additionally, it is well known that aroylhydrazones represent an important group of active molecules having numerous biological properties.<sup>17-20</sup> Challenges in the field of pharmaceutical research are oriented towards discovery of new active pharmaceutical ingredients (APIs) or towards improvement of existing ones. Generally, the imperative is to improve their properties such as solubility, physical stability or mechanical properties.<sup>21,22</sup> Development of novel solid forms such as salts or co-crystals is one of the usual ways to achieve these goals. The main challenge for this concept is selection of an appropriate counter ion, which would afford improved properties of a new solid form.<sup>23</sup> Otherwise, this could be realized by formation of different polymorphs or solvates. Since the existence of various forms cannot be predicted and neither can their properties, researchers are

encouraged to search for alternative solid forms and to fully characterise those forms. The differences between various forms should be explored profoundly taking into account the main intermolecular interactions.

Up to now co-crystals derived from salicylaldehyde isonicotinoyl hydrazone (Salinazid) and dicarboxylic acids or saccharin were obtained and characterized by the single crystal X-ray diffraction method.<sup>24,25</sup> However, scientific reports on inorganic salts are scarce.<sup>26,27</sup> Therefore, in continuation of our studies with this class of compounds,<sup>28-30</sup> within this work we describe formation of the chloride, bromide, nitrate, hydrogen sulfate and sulfate salts of two methoxy-substituted salinazid hydrazones, **L**<sup>1</sup> (4-methoxysalicylaldehyde isonicotinoyl hydrazone) and **L**<sup>2</sup> (3-methoxysalicylaldehyde isonicotinoyl hydrazone), Scheme 1. This part involved optimisation of the experimental conditions for their synthesis. The bulk phase purity of all salts was characterized by powder X-ray diffraction, spectroscopy and thermal techniques.

In this report, we discuss our efforts to improve properties of the selected hydrazones, such as stability and dissolution properties, by preparing their crystalline salts. Additionally, our goal was to investigate the possibility of formation of different polymorphic forms, the influence of nonbonding interactions in the stabilisation of a particular salt form, solid-state properties of different forms, and the propensity for transformation between forms when exposed to different conditions.



**Scheme 1** Molecular structure of the isonazid-based hydrazones  $L^1$  and  $L^2$  (with 4-methoxy and 3-methoxy substituent as R, respectively).

In the end, cytotoxic and antimicrobial activities of the obtained compounds against selected human cancer cell lines and a wide range of clinically important Gram-positive and Gram-negative bacterial strains were assessed. According to the Orange Book list<sup>31</sup> selected counterions may be considered as pharmaceutically relevant. Chloride continues to be the most frequently utilized anionic counterion for the formation of salts.

## Experimental section

### Preparative part

$L^1$  and  $L^2$  were prepared as previously described.<sup>32,33</sup> Methanol, isonicotinyl hydrazine, 3-methoxysalicylaldehyde, 4-methoxysalicylaldehyde, hydrochloric acid (37%), hydrobromic acid (47%), nitric acid (63%) and sulfuric acid (98%) were of reagent grade. Spectral and analytical data for all compounds are given in ESI†.

**Synthesis of  $(HL^1)^+Cl^-$ .** Concentrated hydrochloric acid (37%, 130  $\mu$ L) was added under stirring at 10 °C to a methanolic solution of  $L^1$  (0.09 g, 0.30 mmol in 40 mL). After 1 h of the continuous stirring at 10 °C a yellow product was filtered and dried. The solution was slowly evaporated and after a few days the yellow crystals suitable for X-ray structure analysis were obtained. Yield: 0.06 g; 59 %.

**Synthesis of  $(HL^1)^+Br^-$  ( $\alpha$ ).** Hydrobromic acid (47%, 175  $\mu$ L) was added to a stirred solution of  $L^1$  in methanol (0.09 g, 0.30 mmol in 80 mL) at 10 °C. The temperature was raised to 25 °C and after 1 h of the continuous stirring the solution was heated for 3 hours at 40 °C and then evaporated under vacuum to one-fourth of the initial volume. The resulting orange substance was filtered and dried. Yield: 0.06 g; 51 %.

**Synthesis of  $(HL^1)^+Br^-$  ( $\beta$ ).** Hydrobromic acid (47%, 175  $\mu$ L) was added to a stirred solution of  $L^1$  in methanol (0.09 g, 0.30 mmol in 80 mL) at 10 °C. The temperature was raised to 25 °C and after 1 h of the continuous stirring the solution was heated for 3 hours at 40 °C. The solution was allowed to evaporate slowly at room temperature for a few days. The reaction led to a mixture of forms  $\alpha$  (orange crystals) and  $\beta$  (yellow crystals). Individual crystals of  $\beta$  form were carefully separated manually and used as seeds.

The procedure performed at 10 °C as it is described above was repeated and seeds of  $\beta$  form together with hydrobromic acid were added to the reaction mixture. After 2 h of the continuous stirring at 10 °C the resulting yellow substance was filtered and dried. Yield: 0.05 g; 43 %.

**Synthesis of  $[H(L^1)_2]^+Br^-$ .** Polymorph  $(HL^1)^+Br^-$  ( $\alpha$ ) (0.05 g) was dissolved in methanol (10 mL) at room temperature. The solution was allowed to evaporate very slowly at room temperature for a few days. The resulting yellow crystals of

$[H(L^1)_2]^+Br^-$  were filtered and dried. Yield: 0.04 g; 80%.

**Synthesis of  $(HL^1)^+NO_3^-$ .** Concentrated nitric acid (65 %, 105  $\mu$ L) was added under vigorous stirring at 15 °C to a methanolic solution of  $L^1$  (0.09 g, 0.30 mmol in 80 mL). The temperature was raised to 25 °C and after 1 h of the continuous stirring, the solution was left overnight. The resulting yellow product was filtered and dried. Yield: 0.08 g; 72 %.

**Synthesis of  $(HL^1)^+HSO_4^-$  ( $\alpha$ ).** Sulfuric acid (50 %, 210  $\mu$ L) was added to a stirred solution of  $L^1$  in methanol (0.09 g, 0.30 mmol in 40 mL) at 10 °C. After 1 h of continuous stirring at 10 °C the obtained orange product was filtered and dried. Yield: 0.07 g; 64 %.

**Synthesis of  $(HL^1)^+HSO_4^-$  ( $\beta$ ).** Sulfuric acid (50 %, 210  $\mu$ L) was added to a stirred solution of  $L^1$  in methanol (0.09 g, 0.30 mmol in 80 mL) at 15 °C. The temperature was raised to 25 °C and after 1 h of the continuous stirring, the solution was heated for 3 hours at 40 °C. It was evaporated under vacuum to one-fourth of the initial volume and left in a refrigerator overnight. The resulting yellow substance was filtered and dried. Yield: 0.09 g; 74 %.

**Synthesis of  $(HL^1)_2^{2+}SO_4^{2-}$ .** Sulfuric acid (50 %, 210  $\mu$ L) was added to a stirred solution of  $L^1$  in methanol (0.09 g, 0.30 mmol in 80 mL) at 15 °C. The temperature was raised to 25 °C and after 1 h of the continuous stirring, the solution was allowed to evaporate slowly at room temperature for a few days. The obtained orange crystalline product was filtered and dried. Yield: 0.07 g; 66 %.

**Synthesis of  $(HL^2)^+Cl^- \cdot 0.5H_2O$ .** Concentrated hydrochloric acid (47%, 175  $\mu$ L) was added to a stirred solution of  $L^2$  in methanol (0.09 g, 0.30 mmol in 80 mL) at 10 °C. The temperature was raised to 25 °C and after 1 h of continuous stirring the solution was heated for 3 hours at 40 °C and then evaporated under vacuum to one-fourth of the initial volume. The resulting yellow substance was filtered and dried. Yield: 0.085 g; 79 %.

**Synthesis of  $(HL^2)^+Br^- \cdot MeOH$ .** Hydrobromic acid (47%, 175  $\mu$ L) was added to a stirred solution of  $L^2$  in methanol (0.09 g, 0.30 mmol in 80 mL) at 10 °C. The temperature was raised to 25 °C and after 1 h of the continuous stirring the solution was heated for 3 hours at 40 °C and then evaporated under vacuum to one-fourth of the initial volume. The resulting yellow substance was filtered and dried. Crystals easily lose solvent molecules at room temperature and were analysed as  $(HL^2)^+Br^-$ . Yield: 0.05 g; 42 %.

**Synthesis of  $(HL^2)^+NO_3^-$ .** Concentrated nitric acid (63 %, 105  $\mu$ L) was added under stirring at 15 °C to a methanolic solution of  $L^2$  (0.09 g, 0.30 mmol in 80 mL). The temperature was raised to 25 °C and after 1 h of the continuous stirring the solution was heated for 3 hours at 40 °C and then evaporated under vacuum to one-fourth of the initial volume. The resulting yellow substance was filtered and dried. Yield: 0.084 g; 77 %.

**Synthesis of  $(HL^2)^+HSO_4^- \cdot MeOH$ .** Sulfuric acid (50 %, 210  $\mu$ L) was added under stirring at 15 °C to a methanolic solution of  $L^2$  (0.09 g, 0.30 mmol in 80 mL). The temperature was raised to 25 °C and after 1 h of the continuous stirring, the solution was heated for 3 hours at 40 °C and then evaporated

under vacuum to one-fourth of the initial volume. The resulting yellow substance easily loses methanol molecules at room temperature and was analysed as  $(\text{HL}^2)^+\text{HSO}_4^-$ . Yield: 0.085 g; 70 %.

### 5 Physical methods

Elemental analyses were provided by the Analytical Services Laboratory of the Ruđer Bošković Institute, Zagreb. Thermogravimetric (TG) analyses were performed by using Mettler TG 50 thermobalance with aluminum crucibles.

Differential scanning calorimetry (DSC) measurements were undertaken using Mettler–Toledo DSC823e calorimeter. The results were developed by applying the Mettler STAR<sup>o</sup> 9.01. software. All experiments were recorded in a dynamic atmosphere with oxygen flow rate of  $200 \text{ cm}^3 \text{ min}^{-1}$ .

Attenuated total reflectance Fourier transform infrared spectroscopy (FT-IR – ATR) were performed with a Perkin Elmer Spectrum Two Spectrometer in the  $4500\text{--}450 \text{ cm}^{-1}$  region. All the NMR spectra were recorded on a Bruker Avance 300 NMR spectrometer operating at 300 MHz for  $^1\text{H}$  and 75 MHz for  $^{13}\text{C}$  using a C/H dual 5 mm probe (for more details see ESI†). Solid-state NMR spectra were recorded on Bruker Avance 300 spectrometer equipped with a 4 mm broad band magic angle spinning (MAS) probe. The samples for  $^{13}\text{C}$  CP-MAS spectra were spun at the magic angle with 10 kHz. The spectra were acquired with 9000 scans and repetition delay of 7 seconds. The electronic absorption spectra were recorded on the Analytik Jena Specord 200 spectrophotometer. The measurements were performed in acetonitrile and methanol using quartz cuvettes (1 cm). UV spectra were recorded at different pHs in methanol in the spectral range 600–200 nm applying a  $2 \text{ cm}^{-1}$  of nominal resolution and 128 scans. The spectra were recorded at 22 °C. Multivariate Data Analysis is described in ESI†.

The dissolution rate in water at 25 °C was monitored by a Varian Cary 50 spectrophotometer, equipped with a fiber optic probe with variable optical path length ( $0.2 \leq l/\text{cm} \leq 4$ ). A sample was carefully added into a thermostated cylindrical titration vessel ( $V = 500 \text{ ml}$ , inner diameter  $d = 8 \text{ cm}$  and height  $h = 11 \text{ cm}$ ) filled with 300 mL of water. The absorbance of the sample at 330 nm was recorded automatically (in the range:  $10 \leq \tau/s \leq 25$ ). The samples were stirred at 800 rpm. The placement of the probe inside the vessel was carefully regulated during dissolution.

The powder X-ray diffraction data for qualitative phase analysis were collected by the Panalytical X'Change powder diffractometer in the Bragg-Brentano geometry using  $\text{CuK}\alpha$  radiation. The sample was contained on a Si sample holder. Patterns were collected in the range of  $2\theta = 5\text{--}50^\circ$  with the step size of  $0.03^\circ$  and at 1.5 s per step. The data were collected and visualized using the X'Pert programs Suite.<sup>34</sup>

**X-Ray Crystallography. Powder diffraction.** Crystal structures of  $(\text{HL}^1)^+\text{NO}_3^-$  and  $(\text{HL}^1)^+\text{HSO}_4^-$  ( $\alpha$  and  $\beta$ ) were solved from laboratory X-ray powder diffraction data using direct space approach. The powder X-ray data were collected on a PANalytical Empyrean diffractometer in the focusing capillary transmission geometry with PIXcel<sup>3D</sup> detector, using  $\text{CuK}\alpha$  radiation for  $(\text{HL}^1)^+\text{NO}_3^-$  and  $(\text{HL}^1)^+\text{HSO}_4^-$  ( $\alpha$ ) and

$\text{CuK}\alpha_1$  radiation for  $(\text{HL}^1)^+\text{HSO}_4^-$  ( $\beta$ ). The samples were contained in a 0.5 mm radius borosilicate glass capillary which was rotating during the measurement. Powder patterns were indexed by TREOR<sup>35</sup> and DICVOL04,<sup>36</sup> both embedded in the Panalytical HighScore Software Suite<sup>37</sup> and also by N-TREOR<sup>38</sup> within the EXPO2014 program.<sup>39</sup> The unit cell parameters used for structure solving were refined and the space group confirmed by Pawley fitting in the HighScore Software Suite. Structural models for  $(\text{HL}^1)^+\text{NO}_3^-$  and  $(\text{HL}^1)^+\text{HSO}_4^-$  ( $\alpha$  and  $\beta$ ) were constructed with the aid of the previously determined crystal structure  $(\text{HL}^1)^+\text{Cl}^-$  (atomic coordinates of the cation were taken from  $(\text{HL}^1)^+\text{Cl}^-$  and the corresponding anions  $\text{NO}_3^-$  or  $\text{SO}_4^{2-}$  were added into the starting models). Five internal degrees of freedom were allowed for the cation. The structures were solved by the simulated annealing method, allowing the cation and anion to move independently. Unit cell parameters, scale factors, atomic coordinates and profile parameters of the Pearson VII profile function were refined in the final Rietveld fit through the EXPO2014 program.<sup>39</sup> Crystal structures were refined with restraints on bond lengths and angles as well as with planarity restraints. The final Rietveld plots of  $(\text{HL}^1)^+\text{NO}_3^-$  and  $(\text{HL}^1)^+\text{HSO}_4^-$  ( $\alpha$  and  $\beta$ ) are given in Fig. S1 in ESI†. The crystallographic data are summarised in Table S1 (see ESI†). The reliability factor of refinement  $R_{\text{wp}}$  for  $(\text{HL}^1)^+\text{HSO}_4^-$  ( $\beta$ ) is somewhat higher than one would expect. There are no unexplained diffraction maxima in the experimental data. However, there are differences in intensities of certain diffraction maxima between experimental and calculated powder patterns that can not be explained by preferred orientation or some other physical properties of the measured sample. It is most likely that the intensity differences are caused by an impurity in the sample that is in low concentration and overlapping with the reported polymorph and cannot be clearly identified in the powder pattern.

**X-Ray Crystallography. Single crystal diffraction.** The single-crystal X-ray diffraction data of  $(\text{HL}^1)^+\text{Cl}^-$ ,  $(\text{HL}^1)^+\text{Br}^-$  ( $\alpha$  and  $\beta$ ),  $[\text{H}(\text{L}^1)_2]^+\text{Br}^-$ ,  $(\text{HL}^1)_2^+\text{SO}_4^{2-}$  and  $(\text{HL}^2)^+\text{Br}^- \cdot \text{MeOH}$  were collected by  $\omega$ -scans on an Oxford Diffraction Xcalibur 3CCD diffractometer with graphite-monochromated  $\text{MoK}\alpha$  radiation ( $\lambda = 0.71073 \text{ \AA}$ ). Intensity data for  $(\text{HL}^2)^+\text{NO}_3^-$  were collected from a cryoprotected single crystal at the ELETTRA Synchrotron Light Laboratory, beamline XRD-1 (wavelength,  $\lambda = 0.700 \text{ \AA}$ ), equipped with a Dectris Pilatus 2M detector.<sup>40</sup> Data reduction was performed using the CrysAlis software package.<sup>41</sup> Solution, refinement and analysis of the structures were done using the programs integrated in the WinGX system.<sup>42</sup> All structures were solved by the direct methods using SHELXS.<sup>43,44</sup> The refinement procedure was performed by the full-matrix least-squares method based on  $F^2$  against all reflections using SHELXL.<sup>43,44</sup> The non-hydrogen atoms were refined anisotropically. All hydrogen atoms were located in the difference Fourier maps. Because of poor geometry for some of them they were placed in calculated positions and refined using the riding model an exception was the H atom on N3 in  $[\text{H}(\text{L}^1)_2]^+\text{Br}^-$  which was found in the difference Fourier map but was not refined because it is disordered and its occupancy was set at 0.5. Geometrical calculations were

done using PLATON.<sup>45</sup> Drawings of the structures were prepared using the PLATON and MERCURY programs.<sup>46</sup> The crystallographic data are summarized in Tables S2 and S3.

### Antimicrobial activity

Hydrazones and corresponding salts were evaluated for their *in vitro* antibacterial activity. The tested bacterial isolates were obtained from the culture collection at the American Type Culture Collection (ATCC) (Rockville, MD, USA) and at the Microbiology laboratory, Department of Biology, Faculty of Science, University of Split, Croatia (FNSST). The assays were on the following bacterial strains: antibiotic susceptible Gram-positive bacteria including *Bacillus cereus* ATCC 11778, *Clostridium perfringens* FNSST 4999, *Staphylococcus aureus* ATCC 25923 methicillin-susceptible and *S. aureus* methicillin-resistant (MRSA) and antibiotic resistant Gram-negative bacteria namely *Escherichia coli* FNSST 98, *Klebsiella pneumoniae* FNSST 246, and *Acinetobacter baumannii* FNSST 022.

All strains were grown in lysogenic broth (LB) media while being shaken at 150 rpm for 12 h at 37 °C. Part of the bacterial suspension (100 µL) was transferred to a vial containing 5 mL of LB media and incubated for 2 h at 37 °C to get mid logarithmic phase growth of bacteria. Finally, the bacterial suspension was diluted using a phosphate buffer saline (PBS, pH = 7.2) to achieve 10<sup>5</sup> bacteria/mL. In order to investigate the antimicrobial potential of the hydrazones and corresponding salts, a disc diffusion assay was employed according to the CLSI guidelines. In addition, antimicrobial activities were also tested by a broth microdilution assay in 96 well plates. Cefotaxime and gentamicin were used as standard antibacterial agents (see ESI†).

### Cytotoxicity assay

The cytotoxicity of hydrazone salts was tested on THP-1 (acute monocytic leukemia, ATCC TIB-202) and HepG2 (hepatocellular carcinoma, ATCC HB-8065) human cell lines. Cells were cultured in DMEM/F12 medium (HepG2) or in RPMI 1640 medium (THP-1) supplemented with heat-inactivated 10% fetal bovine serum and 1 % antibiotic/antimycotic solution at 37 °C in a 5 % CO<sub>2</sub> atmosphere and 90 % relative humidity. The cytotoxic effect was analysed using MTS assay.<sup>47</sup> A total of 5 × 10<sup>4</sup> THP-1 or HepG2 cells were cultured overnight in 96-well microtiter plates with appropriate cell medium containing aroylhydrazone salt dissolved in DMSO. In experiments with THP-1 cells concentration range of the tested salts was 10<sup>-4</sup>–100 µmol/L, while the range in those regarding HepG2 cells was 0.8–100 µmol/L. Control wells containing media only, media with tested cell line and 1% DMSO and media with cell line and staurosporine (applied in the 10<sup>-6</sup>–100 µmol/L concentration range) were also included in every experiment. After overnight incubation, MTS reagent (CellTiter<sup>®</sup> Aqueous One Solution Cell Proliferation Assay; Promega) was added and incubation proceeded for additional 6 hours in the case of the THP-1 or 1 hour for the HepG2 cells. The absorbance of the formed purple formazan was measured at 490 nm using a microplate spectrophotometer Perkin Elmer Victor-2. The

average IC<sub>50</sub> value was determined from the cell viability *versus* dose curve with GraphPad Prism software. All experiments were performed in duplicate.

## 60 Results and Discussion

### Synthesis

Two series of isoniazid-based hydrazone salts were obtained by adding an excess of mineral acid (HCl, HBr, HNO<sub>3</sub> or H<sub>2</sub>SO<sub>4</sub>) to a methanolic solution of L<sup>1</sup> or L<sup>2</sup>. Depending on the reaction conditions and starting reagents, salts of different stoichiometries (1:1 or 2:1) and/or polymorphic forms were obtained (Scheme S1). In such a way (HL<sup>1</sup>)<sup>+</sup>X<sup>-</sup> and (HL<sup>2</sup>)<sup>+</sup>X<sup>-</sup> salts where X = Cl, Br, NO<sub>3</sub>, HSO<sub>4</sub>, as well as [H(L<sup>1</sup>)<sub>2</sub>]<sup>+</sup>Br<sup>-</sup> and (HL<sup>1</sup>)<sub>2</sub><sup>2+</sup>SO<sub>4</sub><sup>2-</sup> were obtained. The experimental details are given only for the condition which resulted in the product of the best purity or yield. Compounds (HL<sup>1</sup>)<sup>+</sup>Br<sup>-</sup> and (HL<sup>1</sup>)<sup>+</sup>HSO<sub>4</sub><sup>-</sup> exist in two polymorphic forms. Additionally, when they were dissolved at room temperature in dry methanol they were converted into [H(L<sup>1</sup>)<sub>2</sub>]<sup>+</sup>Br<sup>-</sup> and (HL<sup>1</sup>)<sub>2</sub><sup>2+</sup>SO<sub>4</sub><sup>2-</sup>, respectively. In the case of the nonsolvated forms, the appearance of experimental diffraction patterns is consistent with those simulated for those compounds, (Fig. 1, Fig. S2 see ESI†).

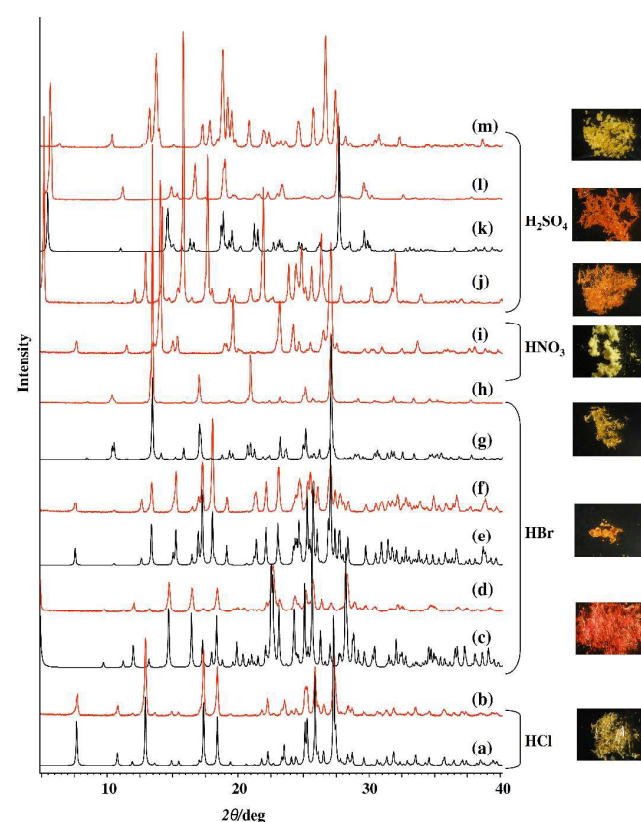


**Fig. 1** PXRD patterns of (HL<sup>1</sup>)<sup>+</sup>Cl<sup>-</sup> (a and b); (HL<sup>1</sup>)<sup>+</sup>Br<sup>-</sup> (α) (c and d); (HL<sup>1</sup>)<sup>+</sup>Br<sup>-</sup> (β) (e and f); [H(L<sup>1</sup>)<sub>2</sub>]<sup>+</sup>Br<sup>-</sup> (g and h), (HL<sup>1</sup>)<sup>+</sup>NO<sub>3</sub><sup>-</sup> (i); (HL<sup>1</sup>)<sup>+</sup>HSO<sub>4</sub><sup>-</sup> (j); (HL<sup>1</sup>)<sub>2</sub><sup>2+</sup>SO<sub>4</sub><sup>2-</sup> (k and l); (HL<sup>1</sup>)<sup>+</sup>HSO<sub>4</sub><sup>-</sup> (β) (m). The orange-red lines indicate patterns obtained by powder diffraction, while the black lines indicate patterns calculated from the X-ray single-crystal structures of the corresponding salts.

The analysis of  $(HL^2)^+X^- \cdot MeOH$  ( $X = Br$  or  $HSO_4$ ) revealed that crystals lose solvent molecules upon standing at room temperature. A sample of the bromide salt showed significant loss of crystallinity, whereas under the same conditions the sulfate salt turned into an amorphous solid.

The hydrazones were stable in presence of strong mineral acids at room temperature and no traces of the starting aldehydes or hydrazine were detected as a result of the hydrolysis.<sup>48</sup> However, it was observed that under different conditions than the ones defined, a mixture of *E* and *Z* isomers was obtained. The <sup>1</sup>H NMR spectra showed two sets of signals with intensity ratio of about 1:0.2 at 298 K (one representative example is given on Fig. S3, see ESI†). This can explain the slow appearance of crystals as expected for molecules that contain rotatable bonds.<sup>49</sup>

All salts are more soluble in water than the parent hydrazone, however, XRPD analysis of the material obtained from an aqueous solution revealed that all salts undergo a dissociation yielding the corresponding hydrazones. Moreover, the dissolution rate of some salts is higher than those obtained for **L**<sup>1</sup> and **L**<sup>2</sup>. Specifically,  $(HL^1)^+HSO_4^-$  (**β** form), and  $(HL^2)^+Cl^- \cdot 0.5H_2O$  and  $(HL^2)^+Br^- \cdot MeOH$  exhibit faster dissolution in comparison to other salt forms (Fig. S4, see ESI†). Additionally, the hydrogen sulfate anion further dissociates in water and there is always some amount of the sulfate ions in the solution. The second dissociation constant of sulfuric acid in aqueous solutions has been the subject of intense investigation over the last decades.

### Thermal stability of salts

As was the case with hydrazones, all compounds, except solvates, remained stable in the solid state for a longer time at ambient conditions, without phase transformations and degradation of the compounds. After two years their PXRD patterns remained unchanged. This property is important for the active pharmaceutical ingredients. A sample of each salt was subjected to DSC analysis. No peaks were observed due to a polymorphic transition.

In all of the cases the melting process was immediately followed by an exothermic peak indicating decomposition. This was additionally confirmed by the TG experiment. One representative example is given on Figure 2. All data are given in ESI†.

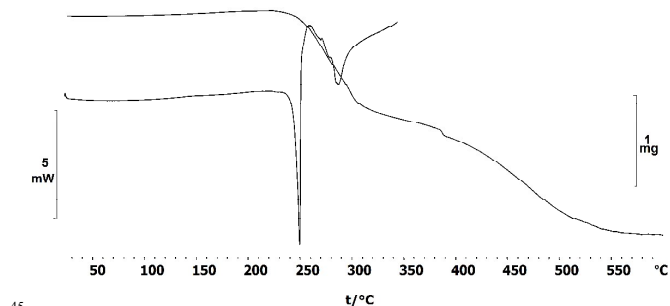


Fig. 2 TG and DSC curves of  $(HL^1)^+Br^-$  (**α**) recorded in a dynamic atmosphere with a flow rate of  $200 \text{ cm}^3 \text{ min}^{-1}$

The salts derived from **L**<sup>1</sup> demonstrated larger thermal stability than the corresponding **L**<sup>2</sup> salts. Interestingly, presence of different anions had a significant impact to the thermal stability altering the melting onset over a significant temperature range ( $\sim 70$  °C). The chloride and bromide salts were more stable in comparison to the corresponding nitrate and hydrogen sulfate salts. The bromide salt  $[H(L^1)_2]^+Br^-$  demonstrated the largest thermal stability and the lowest one was observed for  $(HL^2)^+NO_3^-$ . In comparison to Salinazid salts most of the salts reported here have higher melting points.<sup>24</sup>

### Crystal structures

Analysis of the bond lengths in the cations  $(HL^1)^+$  and  $(HL^2)^+$  from the single crystal data revealed only small or insignificant differences between the investigated crystal structures from those in the corresponding hydrazone<sup>32,33,50</sup> and in the reported  $(HL^2)^+Cl^- \cdot 0.5H_2O$  and  $(HL^2)^+NO_3^-$  structures (Table S4 and S5, see ESI†).<sup>26,27</sup> In all investigated structures the cations  $(HL^1)^+$  or  $(HL^2)^+$  have an *E* configuration with respect to the methylidene unit. The same *E* configuration was found in the corresponding **L**<sup>1</sup> and **L**<sup>2</sup> hydrazones.<sup>32,33,50</sup>

In all investigated crystal structures the cations  $(HL^1)^+$  and  $(HL^2)^+$  have three hydrogen bond donors, the hydroxide-oxygen, hydrazone-nitrogen and the protonated nitrogen atom of the pyridine moiety. The hydroxide-oxygen is also involved in an intramolecular hydrogen bond  $O-H \cdots N$ . The phenyl and pyridyl moieties are not coplanar, the smallest deviation from planarity is in  $(HL^2)^+Br^- \cdot MeOH$  ( $2.55(18)^\circ$ ) and largest in compound  $(HL^1)^+HSO_4^-$  (**α**) being  $13.94^\circ$ . Geometry of hydrogen bonds and geometric parameters of the aromatic stacking interactions are given in Tables S6 and S7, respectively, see ESI†. ORTEP plots of the crystal structures of  $(HL^1)^+Cl^-$ ,  $(HL^1)^+Br^-$  (**α** and **β**),  $[H(L^1)_2]^+Br^-$  and  $(HL^1)_2^+SO_4^{2-}$  are given in ESI†, Fig. S5, while the ORTEP plots of the crystal structures of  $(HL^2)^+Br^- \cdot MeOH$  and  $(HL^2)^+NO_3^-$  are presented in Fig. S6, see ESI†.

#### Crystal structures of compounds with $(HL^1)^+$ cation

**Chloride and bromide salts.** Compounds  $(HL^1)^+Cl^-$  and  $(HL^1)^+Br^-$  (**β**) are isostructural. A common feature of the crystal structures of  $(HL^1)^+Cl^-$  and two polymorphic forms of  $(HL^1)^+Br^-$  (polymorph **α** and **β**) is the association of two  $(HL^1)^+$  cations and two anions ( $Cl^-$  or  $Br^-$ ) into centrosymmetrical discrete dimers by  $N2-H2 \cdots Cl/Br$  and  $N3-H3 \cdots Cl/Br$  hydrogen bonds, graph set notation  $R_4^2(18)$  (Fig. 3a).

The shortest hydrogen bond distance is  $N3-H3 \cdots Cl[1-x, 2-y, 1-z]$  of  $3.0100(14)$  Å in  $(HL^1)^+Cl^-$  (Table S6, see ESI†). Neighboring dimers in  $(HL^1)^+Cl^-$  and  $(HL^1)^+Br^-$  (**β**) are connected by weak  $C-H \cdots O$  ( $O$  is from 4-methoxy and hydroxide groups) and  $C-H \cdots Cl/Br$  hydrogen bonds forming infinite double layers (Fig. 3b). Hydrogen bonds in  $(HL^1)^+Cl^-$  in two selected 2D layers are presented in Fig. S7, ESI†. Such hydrogen-bonded units are linked together by aromatic stacking interaction (Table S7).

In the crystal structure of  $(\text{HL}^1)^+\text{Br}^-$  ( $\alpha$ ) centrosymmetrical discrete dimers are connected by weak interactions of the type C–H $\cdots$ Br and C–H $\cdots$ O (O is from 4-methoxy, carbonyl and hydroxide groups) into a 3D network (Fig. 3c) with a herringbone structural motif (Fig. S8, ESI $\dagger$ ).

In the crystal structure of  $[\text{H}(\text{L}^1)_2]^+\text{Br}^-$  the protonated hydrazone ( $\text{HL}^1$ ) $^+$  cation is connected by the N3–H3 $\cdots$ N3[1-x,y,1/2-z] hydrogen bond of 2.687(2) Å to the neighboring unprotonated hydrazone L $^1$ . Br $^-$  ion links cations/hydrazones by N2–H2 $\cdots$ Br hydrogen bonds of 3.382(2) Å and these interactions give rise to infinite step like chains (Fig. 4). Cations in chains are additionally connected by aromatic stacking interactions (Table S7) and C–H $\cdots$ Br interactions. Neighboring chains are connected by weak C–H $\cdots$ Br and C–H $\cdots$ O<sub>hydroxide</sub> interactions into infinite 2D layers parallel with (100) (Fig. S9, see ESI $\dagger$ ).

**Nitrate salt.** In the crystal structure of  $(\text{HL}^1)^+\text{NO}_3^-$  the nitrate anion links three ( $\text{HL}^1$ ) $^+$  cations through a hydrogen bond with the hydrazone nitrogen atom as the donor (N2–H2 $\cdots$ O5 of 2.888(1) Å) and a bifurcated hydrogen bond involving the pyridine nitrogen atom (N3–H3B $\cdots$ O4[x,1+y,1+z] 2.958(1) Å

and N3–H3B $\cdots$ O4[1-x,2-y,2-z] 2.861(1) Å) forming infinite ribbons along [011]. The combination of these interactions produces  $R_4^4(22)$  motifs (Fig. 5). Additionally, C–H $\cdots$ O<sub>nitrate</sub> interactions within each ribbon are present. Neighboring ribbons are connected by weak C–H $\cdots$ O interactions (oxygen atoms are from hydroxyl and carbonyl groups) into 2D layers (Fig. S10, see ESI $\dagger$ ).

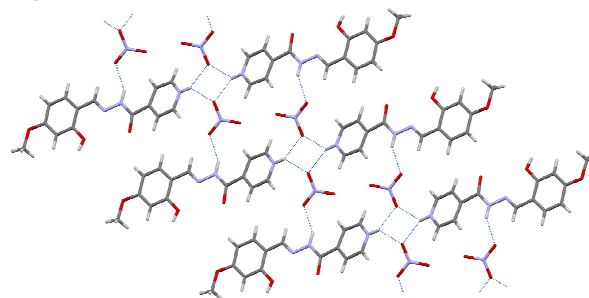


**Fig. 5** Infinite ribbon in  $(\text{HL}^1)^+\text{NO}_3^-$  formed through hydrogen bonds of type N–H $\cdots$ O. Hydrogen bonds are shown by light blue dotted lines.

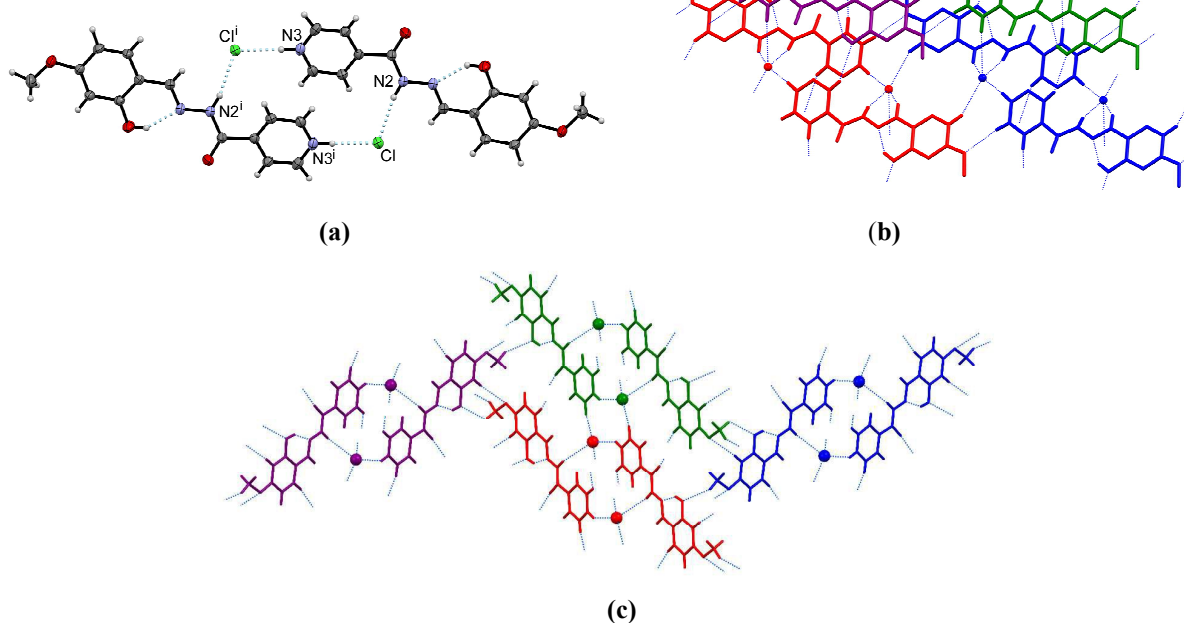


**Fig. 3** (a) Centrosymmetrical dimer formed through N–H $\cdots$ Cl hydrogen bonds in  $(\text{HL}^1)^+\text{Cl}^-$ ; (b) Infinite double layer in  $(\text{HL}^1)^+\text{Cl}^-$ . Four dimers are presented with each discrete dimer shown by different color. Only hydrogen atoms involved in hydrogen bonding are presented; (c) 3D network in  $(\text{HL}^1)^+\text{Br}^-$  ( $\alpha$ ). Four dimers are presented (each discrete dimer is shown by different color). Hydrogen bonds are shown as dashed light blue lines.

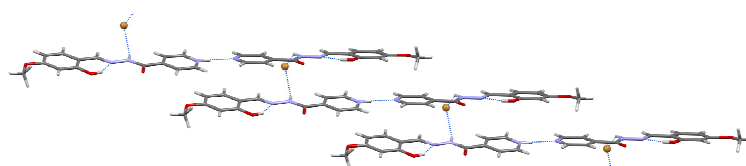


**Fig. 4** Infinite step like 1-D chain in  $[\text{H}(\text{L}^1)_2]^+\text{Br}^-$  formed through hydrogen bonds N–H $\cdots$ N and N–H $\cdots$ Br are shown by light blue dotted lines.

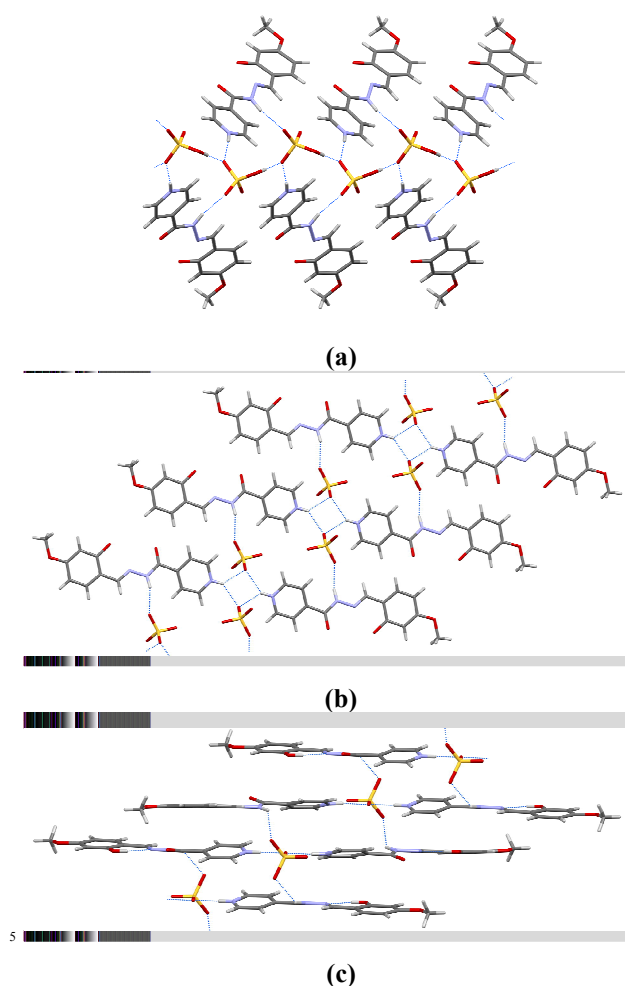


**Fig. 6** (a) Projection of an infinite 2D layer in  $(\text{HL}^1)^+\text{HSO}_4^-$  ( $\alpha$ ) formed through hydrogen bonds of type N–H...O and O–H...O, down the  $b$ -axis; (b) Infinite ribbon in the crystal structure  $(\text{HL}^1)^+\text{HSO}_4^-$  ( $\beta$ ) formed through hydrogen bonds of type N–H...O; (c) Infinite double chain in  $(\text{HL}^1)_2^+\text{SO}_4^{2-}$  formed through hydrogen bonds of type N–H...O. Hydrogen bonds are shown as dashed light blue lines.

**Sulfate and hydrogen sulfate salts.** In the crystal structure of  $(\text{HL}^1)^+\text{HSO}_4^-$  ( $\alpha$ ) each hydrogen sulfate anion is connected with two  $(\text{HL}^1)^+$  cations through the protonated pyridine nitrogen atom and the hydrazone nitrogen atom (N3–H3...O7 of 2.745(1) Å and N2–H2...O4[1/2+x,3/2-y,-1+z] of 2.901(1) Å). Additionally, each hydrogen sulfate anion is linked with two neighboring hydrogen sulfate anions (O5–H2...O7 of 2.613(1) Å) forming infinite 2D layers parallel to (010) (Fig. 6a with a herringbone structural motif (Fig. S11, see ESI†)). Weak C–H...O interactions (oxygen atoms are from hydrogen sulfate and carbonyl groups) are also present within each layer.

In the crystal structure of  $(\text{HL}^1)^+\text{HSO}_4^-$  ( $\beta$ ) each hydrogen sulfate anion is connected with three  $(\text{HL}^1)^+$  cations through the hydrazone nitrogen atom and the protonated pyridine nitrogen atom (N2–H2...O6[-x,-y,-z] of 2.914(1) Å, N3–H3...O7 of 3.0159(1) Å and N3–H3...O7 of 2.8968(1) Å) forming parallel ribbons along the  $b$ -axis (Fig. 6b). This motif,  $R_4^4(22)$  is similar to that in the  $(\text{HL}^1)^+$  nitrate salt. Weak C–H...O<sub>hydrogen sulfate</sub> interactions within each layer are present. Ribbons are connected by weak C–H...O interactions

(oxygen atoms are from the hydroxyl and carbonyl groups) into 2D layers parallel to (001) (Fig. S12, see ESI†).

In the crystal structure of  $(\text{HL}^1)_2^+\text{SO}_4^{2-}$  each sulfate anion links four  $(\text{HL}^1)^+$  cations forming double chains along the  $b$ -axis. One oxygen atom from the sulfate anion is an acceptor of two hydrogen bonds from the protonated pyridinium nitrogen atoms of two cations (N13–H13N...O3S of 2.676(3) Å and N23–H23N...O3S of 2.684(3) Å), while the other two oxygen atoms from the sulfate link two cations through hydrogen bonds involving hydrazone hydrogen atoms (N12–H12N...O1S[-x,3-y,2-z] of 2.931(4) Å and N22–H22N...O2S of 2.769(4) Å (Fig. 6c). Aromatic stacking interactions within the double chains are present (Table S7). Neighboring double chains are connected by weak C–H...O interactions (oxygen atoms are from 4-methoxy, hydroxide and carbonyl group), into a 3D network, Fig. S13, see ESI†. Structural motifs in all investigated compounds are summarised in Table S8. All other interactions are weak dispersion interactions.

#### Crystal structures of compounds with $(\text{HL}^2)^+$ cation

The asymmetric unit of  $(\text{HL}^2)^+\text{Br}^-\cdot\text{MeOH}$  contains a  $(\text{HL}^2)^+$  cation, bromide anion and one methanol molecule of crystallisation. Two cations are linked by  $\text{Br}^-$  through hydrogen bonds involving the pyridine nitrogen atom N3 (N3–H3...Br of 3.209(4) Å) and the hydrazone nitrogen atom N2 (N2–H2...Br [1/2+x,3/2-y,-1/2+z] of 3.482(3) Å) forming infinite zig-zag 1D chains along the  $b$ -axis. The methanol molecule is linked to the  $\text{Br}^-$  anion by the hydrogen bond O4–H4O...Br of 3.325(3) Å (Fig. 7). A weak C7–H7...Br interaction is present within each chain. Neighboring chains are connected into a 3D network by aromatic stacking interactions (Table S7) and weak C–H...O hydrogen bonds (the oxygen atom is from the methanol molecule, hydroxide and carbonyl groups, Fig. S14, see ESI†).

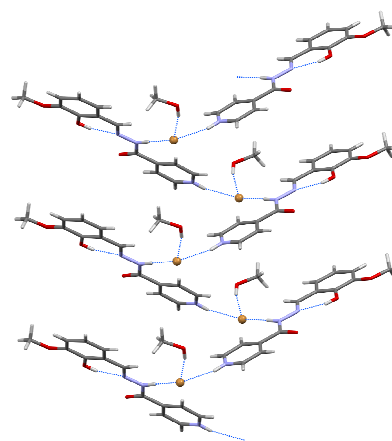


**Fig. 7** Infinite 1D zig-zag chain in  $(\text{HL}^2)^+\text{Br}^-\cdot\text{MeOH}$  formed through hydrogen bonds of type N–H...Br and O–H...Br. Hydrogen bonds are shown by blue dotted lines.

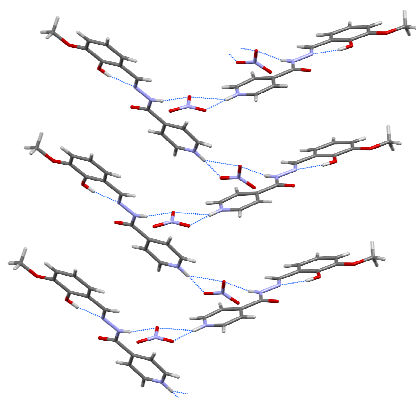


**Fig. 8** Infinite 1D zig-zag chain in one symmetry-independent cation and anion pair of  $(\text{HL}^2)^+\text{NO}_3^-$  formed through hydrogen bonds of type N-H...O. Hydrogen bonds are shown as dashed light blue lines.

The asymmetric unit of  $(\text{HL}^2)^+\text{NO}_3^-$  contains two symmetry-independent  $(\text{HL}^2)^+$  cations and two nitrate anions. Each symmetry-independent cation and anion pair is linked by hydrogen bonds through the pyridine nitrogen atom N3 and hydrazone nitrogen atom N2 to nitrate oxygen atoms forming infinite helical chains around the  $2_1$  axis. (Fig. 8 and Table S6, see ESI†). The chains are connected into a 3D network by aromatic stacking interactions (Table S7) and weak C-H...O hydrogen bonds (Fig. S15, see ESI†). All other interactions are weak dispersion interactions. Structural motifs are summarised in Table S8.

In a recent paper by Surov *et al.*<sup>21</sup> crystal structures of Salinazid with some dicarboxylic acids and acetsulfame are described. It was found that the hydrogen bonds were of different connectivity and complexity as in the present paper. In the salinazid salts with dicarboxylic acids, the acid molecules tend to interact with each other since only one carboxylic group interacts with protonated salinazide. We have found such connectivity only in the structure of  $(\text{HL}^1)^+\text{HSO}_4^-$  ( $\alpha$ ). The  $\text{HSO}_4^-$  salts are distinct from the others since the anions are protonated and can form hydrogen bonds with each other.

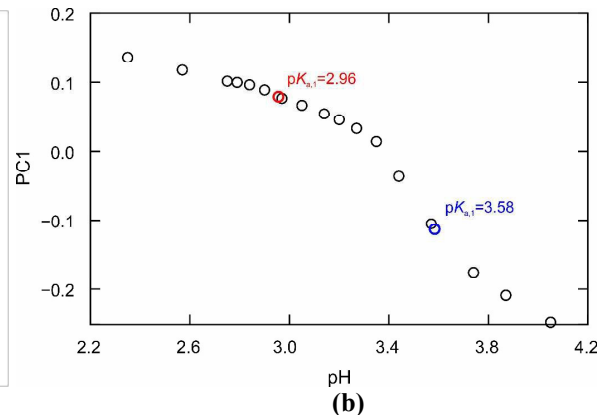
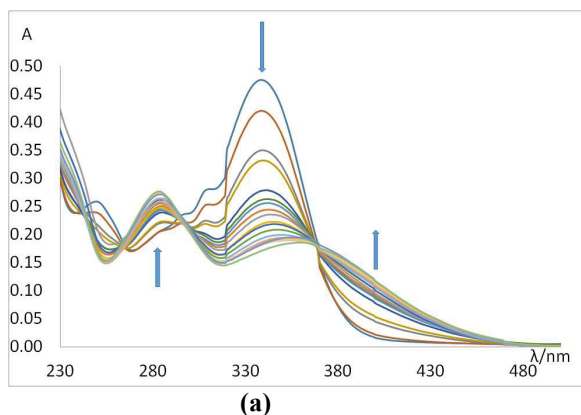


**Fig. 9** (a) The UV/Vis spectra of  $\text{L}^1$  upon addition of HCl in methanol. (b) PC1 scores calculated by principal component analysis performed for a set of UV/Vis spectra of  $\text{L}^1$  in methanol ( $\text{pK}_a$  values were determined by nonlinear regression on generalized logistic curve). A slight discontinuity in spectra around 320 nm is due to the radiation source change.

**FT-IR ATR.** Spectrum of  $\text{L}^1$  showed a strong peak at  $1680 \text{ cm}^{-1}$ , assigned to the carbonyl stretching vibration. Carbonyl bond stretching vibration is shifted to  $1684 \text{ cm}^{-1}$  in  $(\text{HL}^1)^+\text{Cl}^-$ , to  $1682 \text{ cm}^{-1}$  in  $(\text{HL}^1)^+\text{Br}^-$  ( $\alpha$ ), to  $1677 \text{ cm}^{-1}$  in  $(\text{HL}^1)^+\text{NO}_3^-$  and to  $1678 \text{ cm}^{-1}$  in  $(\text{HL}^1)^+\text{HSO}_4^-$  ( $\alpha$ ). In the spectra of  $(\text{HL}^1)^+\text{X}^-$ , several peaks in the range from  $2400$  to  $2000 \text{ cm}^{-1}$  that can be assigned to the aromatic and protonated tertiary amine groups are found. Stretching vibration found at  $1600 \text{ cm}^{-1}$  is assigned to C=N in  $\text{L}^1$  and is shifted for  $\approx 50 \text{ cm}^{-1}$  in all protonated forms.

Spectra of  $(\text{HL}^1)^+\text{HSO}_4^-$  ( $\alpha$ ),  $(\text{HL}^1)^+\text{HSO}_4^-$  ( $\beta$ ) and  $(\text{HL}^1)_2^{2+}\text{SO}_4^{2-}$ , showed similar absorption peaks. Carbonyl bond stretching vibration is at  $1678 \text{ cm}^{-1}$  in  $(\text{HL}^1)^+\text{HSO}_4^-$  ( $\alpha$  and  $\beta$ ) whereas in  $(\text{HL}^1)_2^{2+}\text{SO}_4^{2-}$  it can be found at the lower wavenumber  $1668 \text{ cm}^{-1}$ . FT-IR spectra of  $\text{L}^2$  protonated forms showed similar absorption peaks and trends as in  $\text{L}^1$  series.

**UV/Vis spectroscopy.** We have chosen UV/Vis spectroscopy for further studies in solution in organic solvents. The obtained results clearly show that  $\text{L}^1$  salts upon dissolving in methanol ( $c = 1 \times 10^{-5} \text{ mol dm}^{-3}$ ) completely dissociate into the free hydrazone. However, in acetonitrile, different spectra for the hydrazone and its salts are obtained (Fig. S16, see ESI†). It can be seen that spectra for HCl and  $\text{HNO}_3$  salts are quite close by shape indicating the existence of similar structural elements.

Furthermore, titrations were performed by adding aliquots of HCl into the methanolic solution of the corresponding hydrazone followed by spectrum measuring (Fig. 9 and Fig. S17, respectively). Used absorbance intensities of studied compounds were proportional to their concentrations under the experimental conditions.  $\text{pK}_a$  were calculated by processing titration data (complete spectra) with PCA analysis (Multivariate Data Analysis is described in ESI†). Two  $\text{pK}_a$  values were determined for each hydrazone investigated in methanol, the first relating to the pyridine ring protonation ( $3.6$ ) and the second for the protonation of the imine nitrogen atom ( $2.9$ ). This result is in the agreement with the  $\text{pK}_a$  value based on pyridine nitrogen for salinazid ( $3.6$ ).<sup>24</sup>

When titrations were performed by adding aliquots of acid in DMSO the corresponding  $pK_a$  values were 2.57 and 1.81 for  $L^1$  and 2.79 and 1.92 for  $L^2$  (Fig. S18 and Fig. S19, see ESI†). The  $pK_a$  value for  $HSO_4^-$  in DMSO is high (14.7 at 25 °C), indicating that  $HSO_4^-$  ion is highly stabilized in solution, presumably by strong intermolecular hydrogen bonding in aprotic solvents.<sup>51,52</sup> It is expected that all other salts are dissociated under the experimental conditions described above.

**NMR spectroscopy.** The proton and carbon chemical shifts were assigned by using one- and two- dimensional NMR techniques (Tables S9 and S10, Scheme S2 see ESI†). Downfield shifts and wide line widths of NH and OH protons indicated presence of hydrogen bonding interactions, Fig. S20, see ESI†. NH groups exhibited proton signals in the range 12.003 to 12.964 ppm. Chemical shifts of amide C=O group of all compounds were observed in the range 159.90-161.94 ppm which is similar to the values obtained for the solid samples.

Observed changes in NMR chemical shifts pointed towards protonation of the nitrogen atom in the pyridine ring, which was also observed in the solid state. The largest changes were detected for hydrogens at positions 2 and 5 in the pyridine ring. The pyridine protons and carbons at positions 3 and 4 were found between 8.823 and 9.094 ppm and 149.84 and 151.03 ppm, respectively. Singlets in the range 3.770 to 3.824 ppm were assigned to methyl protons. OH protons in the benzene ring were shifted to both higher and lower ppm values in the salts as a consequence of changes in hydrogen bonding interactions in which these protons participate, and the influence of counter ions. In line with this observation is the shielding effect of ca 6 ppm at C7 atom. <sup>13</sup>C chemical shift assignment in the solid state was made on the basis of comparison with chemical shifts observed in solution (Fig. S21, Table S11, see ESI†).

## Antimicrobial evaluation

Initial antimicrobial profiling of the both hydrazones  $L^1$  and  $L^2$ , and their salts  $(HL^1)^+X^-$  and  $(HL^2)^+X^-$  was performed to provide an assessment of their efficacy against a diverse panel of selected antibiotic susceptible and resistant Gram-positive and Gram-negative bacteria by disc diffusion assay. The tested samples were dissolved in DMSO to prepare a stock solution (see ESI†).<sup>53</sup> As shown in Table S12 (see ESI†), all compounds displayed a variable degree of antimicrobial activity against all the strains tested, with respective diameter zones of inhibition. The mean zones of inhibition of the target compounds against all the bacterial strains tested were found in the range of  $9.7 \pm 1.2$  to  $26.5 \pm 1.1$  mm.

The antimicrobial activity was investigated also by a broth microdilution method based on the minimum inhibitory concentrations (MICs). The results presented in Table 1 revealed that all of the tested compounds showed selectivity and antimicrobial activities with MIC values in range  $0.39$ - $125 \mu\text{g mL}^{-1}$ . The hydrazones showed better inhibitory potency than corresponding salts and some of them were much more active than gentamicin and cefotaxime.

Moreover,  $L^1$  and  $L^2$  were more active against the Gram-negative than against Gram-positive bacteria, except for *S. aureus*. Especially,  $L^1$  exhibited 8- and 4-fold more activity against MRSA with lower concentration than gentamicin and cefotaxime, respectively. Also,  $L^1$  showed notable inhibitory profiles against *E. coli* and *A. baumannii*, 5-fold lower than gentamicin. Similarly,  $L^2$  was also found to be more active against *S. aureus* (MRSA) and *E. coli* as well as *A. baumannii*, but had poor activity or was completely inactive against some tested Gram-positive strains.

According to the results (Table 1), the corresponding salts displayed a variable and slightly lesser degree of antimicrobial activity than  $L^1$  and  $L^2$ , respectively. The MIC values of these salts varied with the microbial strains tested, ranging from  $0.39$  to  $125 \mu\text{g mL}^{-1}$ .

**Table 1** Minimum inhibitory concentration of the hydrazones and their salts against a panel of Gram-positive and Gram-negative antibiotic susceptible and resistant strains

Compound	MIC / $\mu\text{g mL}^{-1}$						
	Gram-positive bacteria				Gram-negative bacteria		
	<i>B. cereus</i>	<i>C. perfringens</i>	<i>S. aureus</i>	<i>S. aureus</i> MRSA	<i>E. coli</i>	<i>K. pneumoniae</i>	<i>A. baumannii</i>
$L^1$	50	125	1.56	1.56	6.25	25	0.78
$(HL^1)^+Cl^-$	100	50	25	12.5	25	50	1.56
$(HL^1)^+Br^-^a$	50	125	12.5	0.78	6.25	25	12.5
$(HL^1)^+NO_3^-$	100	25	25	25	25	25	6.25
$(HL^1)^+HSO_4^-^a$	125	12.5	50	25	50	25	12.5
$L^2$	50	25	50	6.25	6.25	12.5	3.12
$(HL^2)^+Cl^- \cdot 0.5H_2O$	50	50	0.78	0.39	25	6.25	6.25
$(HL^2)^+Br^-$	100	25	50	25	25	6.25	6.25
$(HL^2)^+NO_3^-$	25	50	25	0.78	12.5	3.12	12.5
$(HL^2)^+HSO_4^-^b$	12.5	125	50	25	25	25	25
Gentamicin	6.25	6.25	1.56	12.5	25	6.25	50
Cefotaxime	0.78	0.78	0.78	6.25	6.25	0.78	25

<sup>a</sup>  $\alpha$  form is tested. <sup>b</sup> Unsolvated form

Generally, the salts had similar selectivity as their parent hydrazones. The salts derived from  $L^1$  showed a substantially

lower activity than the corresponding salts of  $L^2$ , suggesting that the position of the methoxy functional group influences the antimicrobial activities. Additionally, the presence of anions like chloride, bromide and nitrate significantly enhances the antimicrobial potential. This may be due to the different interactions with membrane components. The  $(HL^1)^+HSO_4^-$  or  $(HL^2)^+HSO_4^-$  salts show poor to moderate antibacterial activity at the tested conditions.

The most promising antimicrobial potential against a panel of multidrug resistant strains such as *S. aureus* (MRSA), *E. coli*, *K. pneumoniae*, *A. baumannii* was observed for  $(HL^2)^+NO_3^-$ . The nitrate formed from the  $L^1$  has shown smaller activity. Similarly, the chloride salts formed from the  $L^2$  also displayed appreciable activity on the *S. aureus*, *S. aureus* (MRSA), *K. pneumoniae* and *A. baumannii*. It should be noted that among multidrug Gram-negative bacteria tested *A. baumannii* was found to be more susceptible to all salts tested with MIC values in range 1.56-25  $\mu\text{g mL}^{-1}$ . *A. baumannii* is the leading nosocomial pathogen worldwide resistant to virtually all clinically useful antibiotics.

### Cytotoxicity

$IC_{50}$  values of aroylhydrazone salts determined by the MTS test are given in Table 2. The concentrations of compounds required for 50 % decrease in cell viability, i.e.  $IC_{50}$  values, higher than 100  $\mu\text{mol/L}$  indicate that all examined compounds are noncytotoxic against HepG2 cell line while their weak cytotoxicity was established on THP-1 cells.

When considering the effect of the anion on the cytotoxic activity against THP-1, it can be seen that the cytotoxicity changes only slightly with the anion exchange in each of the hydrazone salt series. Comparing the cytotoxicity of hydrazone  $L^1$  and its salts, no significant difference is observed. Even though the cytotoxicity differences observed for hydrazone  $L^2$  and its salts are likewise small it can still be noted that the salts have lower cytotoxic activity than  $L^2$ . Furthermore, each salt  $(HL^2)^+X^-$  has somewhat higher cytotoxic activity than the corresponding  $(HL^1)^+X^-$ . Also, the same trend is found for the parent hydrazones  $L^2$  and  $L^1$ .<sup>54</sup>

**Table 2** The  $IC_{50}$  values for aroylhydrazones and their salts

Compound	$IC_{50}/\mu\text{mol L}^{-1}$	
	THP-1	HepG2
$L^1$	37.81	>100
$(HL^1)^+Cl^-$	39.03	>100
$(HL^1)^+Br^-^a$	27.88	>100
$(HL^1)^+NO_3^-$	46.50	>100
$(HL^1)^+HSO_4^-^a$	36.09	>100
$L^2$	11.61	>100
$(HL^2)^+Cl^- \cdot 0.5H_2O$	26.85	>100
$(HL^2)^+Br^-$	23.99	>100
$(HL^2)^+NO_3^-$	15.87	>100
$(HL^2)^+HSO_4^-^b$	27.27	>100
Staurosporine	0.50	2.58

<sup>a</sup>  $\alpha$  form is tested. <sup>b</sup> Unsolvated form.

## Conclusion

Diversity in the formation of salinazid-based salts illustrates their sensitivity to the reaction conditions. Two categories of salts were obtained:  $HL^+$  with  $X^{n-}$  ( $n = 1$  or  $2$ ) in ratios 1:1 and 2:1 ratio. Up to now, data on different salts and/or polymorphs based on aroylhydrazone with this type of acids are quite rare. In all salts, the pyridyl moiety of the corresponding hydrazone is found to be protonated exhibiting different hydrogen bonding to halides ( $Cl^-$  and  $Br^-$ ), and oxyanions ( $NO_3^-$ ,  $HSO_4^-$  and  $SO_4^{2-}$ ). Strong hydrogen bonds of the type  $N-H \cdots A$  (N from pyridine and hydrazone moiety of hydrazone; A = acceptor atom from anion) are present in all structures forming different primary building units: (i) dimers, (ii) chains or ribbons and (iii) layers.

A change of anion or methoxy substituent position proves to be a useful tool to obtain salts of different connectivities, thermal stabilities and properties. All salts were found to be stable in the solid state for a longer time at ambient conditions, without phase transformations and degradation of the compounds. The hydrazone salts are more soluble than parent hydrazones. However, upon dissolution in water they interconvert into the corresponding hydrazones.

The antimicrobial profiles of the presented salts demonstrated a high potential for expansion and further optimization of this type of compounds as promising antimicrobial agents including multidrug-resistant Gram-negative bacterial strains, especially *Acinetobacter baumannii*, as emerging pathogens. All investigated salts were found to be noncytotoxic on HepG2 and showed only weak cytotoxic activity on THP-1 cells.

## Conflict of interest

There are no conflicts to declare.

## Acknowledgments

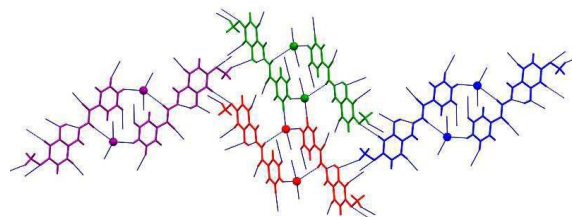
This work has been fully supported by Croatian Science Foundation under the project IP-2016-06-4221. We are grateful to Alberto Cassetta and Nicola Demitri for valuable support during beamtime at Elettra synchrotron. We are grateful to Katarina Leko for help with dissolution rate measurements.

## Notes and references

- <sup>a</sup> University of Zagreb, Faculty of Science, Department of Chemistry, Horvatovac, 102a, 10000 Zagreb, Croatia, Fax: ++ 385-1-4606341; Tel: ++385-1-4606353; E-mail: visnja.vrdoljak@chem.pmf.hr
- <sup>b</sup> Department of Chemistry and Biochemistry, School of Medicine, University of Zagreb, Šalata 3, 10 000 Zagreb Croatia
- <sup>c</sup> INA-Industrija nafte d.d., Refining & marketing business division, Product development department, Lovinčičeva bb, 10002 Zagreb, Croatia
- <sup>d</sup> Department of Chemistry, Faculty of Science, University of Split, Ruđera Boškovića 33, 21000 Split, Croatia
- <sup>e</sup> Department of Biology, Faculty of Science, University of Split, Ruđera Boškovića 33, 21000 Split, Croatia
- <sup>f</sup> Malvern Analytical B.V., Lelyweg 1, 7602 EA Almelo, The Netherlands

† Electronic Supplementary Information (ESI) available: 1) powder diffraction patterns, (2) spectral data, (3) single crystal X-ray diffraction data, (4), figures for compounds, (5) yields and analytical data, (6) UV-

- Vis and NMR spectral data, (7) Experimental details biological activity testings. Crystallographic data sets for the structures are available through the Cambridge Structural Data base with deposition numbers CCDC 1589824 – 1589831. See DOI: 10.1039/b000000x/
- 5 1 M. Hidai and Y. Mizobe, *Chem. Rev.*, 1995, **95**, 1115.
  - 2 R. Lazny and A. Nodzevska, *Chem. Rev.*, 2010, **110**, 1386.
  - 3 S. Kobayashi, Y. Mori, J. S. Fossey and M. M. Salter, *Chem. Rev.*, 2011, **111**, 2626.
  - 4 P. Vicini, F. Zani, P. Cozzini and I. Doytchinova, *Eur. J. Med. Chem.*, 2002, **37**, 553.
  - 5 C. Loncle, J. M. Brunel, N. Vidal, M. Dherbomez and Y. Letourneux, *Eur. J. Med. Chem.*, 2004, **39**, 1067.
  - 6 L. Savini, L. Chiasserini, V. Travagli, C. Pellerano, E. Novellino, S. Cosentino and M. Pisano, *Eur. J. Med. Chem.*, 2004, **39**, 113.
  - 7 J.-M. Lehn, *Chem. Soc. Rev.*, 2007, **36**, 151.
  - 8 J.-M. Lehn, *Angew. Chem., Int. Ed.*, 2013, **52**, 2836.
  - 9 F. J. Uribe-Romo, C. J. Doonan, H. Furukawa, K. Oisaki and O. M. Yaghi, *J. Am. Chem. Soc.*, 2011, **133**, 11478.
  - 10 D. N. Bunck and W. R. Dichtel, *J. Am. Chem. Soc.*, 2013, **135**, 14952.
  - 11 J.-M. Lehn, *Chem.-Eur. J.*, 2006, **12**, 5910.
  - 12 S. M. Landge and I. Aprahamian, *J. Am. Chem. Soc.*, 2009, **131**, 18269.
  - 13 S. M. Landge, E. Tkatchouk, D. Benitez, D. A. Lanfranchi, M. Elhabiri, W. A. Goddard and I. Aprahamian, *J. Am. Chem. Soc.*, 2011, **133**, 9812.
  - 14 D. Ray, J. T. Foy, R. P. Hughes and I. Aprahamian, *Nat. Chem.*, 2012, **4**, 757.
  - 15 X. Su, T. F. Robbins and I. Aprahamian, *Angew. Chem., Int. Ed.*, 2011, **50**, 1841.
  - 16 A. D. Mitchel and D. C. Nonhebel, *Tetrahedron Lett.*, 1975, **16**, 3859.
  - 17 N. Belkheri, D. Bougerne, F. Bedos-Beval, H. Duran, C. Bernis, R. Salvayre, A. Nègre-Salvayre and M. Baltas, *Eur. J. Med. Chem.*, 2010, **45**, 3019.
  - 18 G. Verma, A. Marella, M. Shaquiquzzaman, M. Akhtar, M. R. Ali and M. M. Alam, *J. Pharm. Bioall. Sci.*, 2014, **6**, 69.
  - 19 S. Rollas and Ş. Güniz Küçükgül, *Molecules*, 2007, **12**, 1910.
  - 20 R. Dabideen, K. F. Cheng, B. Aljabari, E. J. Miller, V. A. Pavlov and Y. Al-Abed, *J. Med. Chem.*, 2007, **50**, 1993.
  - 21 J. Haleblan and W. McCrone, *J. Pharm. Sci.* 1969, **58**, 11.
  - 22 R. Hilfiker, F. Blatter and M. von Raumer, In *Polymorphism: in the Pharmaceutical industry*; R. Hilfiker, Ed.; Wiley-VCH Verlag GmbH & Co.: Weinheim, Germany, 2006; pp 1–19.
  - 23 G. S. Paulekuhn, J. B. Dressman and C. Sall, *J. Med. Chem.*, 2007, **50**, 6665.
  - 24 A. O. Surov, A. P. Voronin, A. A. Simagina, A. V. Churakov and G. L. Perlovich, *Cryst. Growth Des.*, 2016, **16**, 2605.
  - 25 A. O. Surov, A. P. Voronin, A. A. Simagina, A. V. Churakov, S. Y. Skachilova and G. L. Perlovich, *New J. Chem.*, 2015, **39**, 8614.
  - 26 M. Tabatabaee, A. Taghinezhadkoshknou, M. Dušek and K. Fejfarova, *Synth. React. Inorg., Met.-Org., Nano-Met. Chem.*, 2015, **45**, 1506.
  - 27 S.-W. Chen, H.-D. Yin, D.-Q. Wang, X. Kong and X.-F. Chen, *Acta Crystallogr., Sect. E: Struct. Rep. Online*, 2006, **62**, o2043.
  - 28 V. Vrdoljak, B. Prugovečki, D. Matković-Čalogović, R. Dreos, P. Siega and C. Tavagnacco, *Cryst. Growth Des.*, 2010, **10**, 1373.
  - 29 V. Vrdoljak, B. Prugovečki, D. Matković-Čalogović, J. Pisk, R. Dreos and P. Siega, *Cryst. Growth Des.*, 2011, **11**, 1244.
  - 30 V. Vrdoljak, B. Prugovečki, D. Matković-Čalogović, T. Hrenar, R. Dreos and P. Siega, *Cryst. Growth Des.*, 2013, **13**, 3773.
  - 31 U.S. Food and Drug Administration Orange Book.  
<http://www.fda.gov/cder/ob/>.
  - 32 M. Yu, X. Chen and Z.-L. Jing, *Acta Crystallogr. Sect. E: Struct. Rep. Online*, 2005, **61**, o1345.
  - 33 F. Zhi and R. Wang, *Acta Crystallogr. Sect. E: Struct. Rep. Online*, 2010, **66**, o892.
  - 34 X'Pert Software Suite, Version 1.3e; Panalytical B. V., Almelo, The Netherlands, 2001.
  - 35 P. E. Werner, L. Erikson and M. Westdahl, *J. Appl. Cryst.*, 1985, **18**, 367.
  - 36 A. Boultaf and D. Louër, *J. Appl. Cryst.*, 2004, **37**, 724.
  - 37 T. Degen, M. Sadki, E. Bron, U. König and G. Nénert, *Journal of Powder Diffraction*, 2014, **29**, Supplement S2, S13.
  - 38 A. Altomare, C. Giacovazzo, A. Guagliardi, A. G. G. Moliterni, R. Rizzi and P.-E. Werner, *J. Appl. Cryst.*, 2000, **33**, 1180.
  - 39 A. Altomare, C. Cuocci, C. Giacovazzo, A. Moliterni, R. Rizzi, N. Corriero and A. Falcicchio, *J. Appl. Cryst.*, 2013, **46**, 1231.
  - 40 A. Lausi, M. Polentarutti, S. Onesti, J. R. Plaisier, E. Busetto, G. Bais, L. Barba, A. Cassetta, G. Campi, D. Lamba, A. Pifferi, S. C. Mande, D. D. Sarma, S. M. Sharma and G. Paolucci, *Eur. Phys. J. Plus*, 2015, **130**, 1.
  - 41 CrysAlisPro Software System, Version 1.171.38.41; Rigaku Oxford Diffraction, 2015.
  - 42 L. J. Farrugia, *J. Appl. Crystallogr.*, 2012, **45**, 849.
  - 43 G. M. Sheldrick, *Acta Crystallogr., Sect. A: Found. Crystallogr.*, 2008, **64**, 112.
  - 44 G. M. Sheldrick, *Acta Crystallogr.*, 2015, **C71**, 3.
  - 45 A. L. Spek, *Acta Crystallogr., Sect. D: Biol. Crystallogr.*, 2009, **65**, 148.
  - 46 C. F. Macrae, I. J. Bruno, J. A. Chisholm, P. R. Edgington, P. McCabe, E. Pidcock, L. Rodriguez-Monge, R. Taylor, M. Towler, J. Van der Streek and P. A. Wood, *J. Appl. Cryst.*, 2008, **41**, 466.
  - 47 T. Mosmann, *J. Immunol. Methods*, 1983, **65**, 55.
  - 48 B. Levrand, Y. Ruff, J. M.-M. Lehn and A. Herrmann, *ChemComm*, 2006, 2965.
  - 49 A. Samie, G.R. Desiraju, and Manas Banik, *Cryst. Growth Des.*, 2017, **17**, 2406.
  - 50 S.-J. Peng and H.-Y. Hou, *Acta Crystallogr.*, 2008, **E64**, o1996.
  - 51 K. Izutsu, *Electrochemistry in Nonaqueous Solutions*, Wiley-VCH Verlag GmbH & Co.: Weinheim, Matsumoto, Japan, 2002; pp 59–82.
  - 52 S. O. Kang, J. M. Oh, Y. S. Yang, J. C. Chun, S. Jeon and K. C. Nam, *Bull. Korean Chem. Soc.*, 2002, **23**, 145.
  - 53 National Committee for Clinical Laboratory Standards (NCCLS), *Performance Standards for Antimicrobial Susceptibility Testing*, 27th Ed, M100, Wayne, PA, 2017.
  - 54 J. Pisk, T. Hrenar, M. Rubčić, G. Pavlović, V. Damjanović, J. Lovrić, M. Cindrić and V. Vrdoljak, *CrystEngComm*, 2018, **20**, 1804.

**Table of contents entry**

A change of anion or aroylhydrazone substituent position results in salts of different connectivities, thermal stabilities and properties.